RARE EARTH DOPED NANOPARTICLES IN ORGANIC AND INORGANIC HOST MATERIALS FOR APPLICATION IN INTEGRATED OPTICS.

R. Dekker [1)], L.T.H. Hilderink [1)], M.B.J. Diemeer [1)],
J.W. Stouwdam [2)], V. Sudarsan [2)], F.C.J.M. van Veggel [2)], K. Wörhoff [1)],
and A. Driessen [1)].

[1)]University of Twente, Faculty of Electrical Engineering, Mathematics and Computer Science, P.O.Box 217, 7500 AE Enschede, The Netherlands. Phone: +31-53-489 4440; E-mail: R.Dekker@utwente.nl.

[2)]University of Victoria, Department of Chemistry, P.O. Box 3065,Victoria, BC Canada V8W 3V6.

The preparation and the optical properties of lanthanum fluoride (LaF_3) nanoparticles doped with erbium and neodymium will be discussed. Organic and inorganic materials in the form of polymers and sol-gels were used to serve as the hosts for the inorganic nanoparticles, respectively. The organic host material has been synthesized such that it is photo-crosslinkable to facilitate straightforward multimode and monomode waveguide fabrication. Our focus will be on the optical properties of both the inorganic rare-earth doped nanoparticles and the host materials. The importance of the refractive indices of the particles and the host material and particle size on the optical scattering properties will be addressed. The optical transmission windows of the host materials do overlap with the absorption peaks of the erbium and neodymium in order to have efficient optical pumping, as well as with the spontaneous emission spectra of the rare earth metals for use as optical amplifiers around 1330nm and 1550nm. Furthermore, the improvement on the excited state lifetimes of the rare earths in the nanoparticles compared to the lifetimes of rare earths directly immersed in sol-gels will be presented.

INTRODUCTION

The active optical properties of the rare earth ions erbium and neodymium are used to amplify the optical signals used in telecommunication systems around 1550nm (1) and 1330nm, respectively. This amplification takes place through a mechanism called stimulated emission. The trivalent erbium or neodymium ion is pumped with a high power laser into an excited state where it will stay for a relatively long time (millisecond range), until a signal photon passes and triggers the excited ion to fall back to its ground state energy level, emitting a photon with exact the same wavelength, direction and phase as the incoming signal photon. A lot of effort has been put in incorporating erbium and neodymium in integrated optical devices, in order to compensate for the on chip optical losses or to achieve strong non-linear behavior to facilitate all-optical functions like, for instance, switching or modulation. The efficiency of the rare earth elements depends partly on the excited state lifetime of the ions, which strongly depends on the local environment. A broad range of host materials, like SiO_2, Al_2O_3 and LaF_3 have proven to be successful for use in optical amplifiers. However, deposition of these glassy and ceramic materials is time consuming and expensive. Furthermore, etching of micron sized waveguide structures into these, often inert, materials is not straightforward and

expensive as well. The use of low cost photosensitive polymers or sol-gel based materials would enhance the ease of processing and drastically reduce the costs, since the thin films can easily be spin-coated onto a wafer. However, the CH and OH bonds that are always present in these materials are strong energy quenchers of the rare earth ions, resulting in very short excited state lifetimes, decreasing the probability to generate stimulated emitted photons. We combined the properties of both the inorganic and organic material systems by synthesizing erbium and neodymium doped LaF_3 nanoparticles that can be dispersed in photosensitive polymer and sol-gel solutions. The resulting hybrid materials can be spin-coated onto a sample, followed by a UV-exposure and development step to fabricate optically active multimode and monomode waveguides (2).

EXPERIMENTAL

Nanoparticle preparation.

Two types of rare earth doped LaF_3 nanoparticles have been synthesized, *i.e.* cyclopentanone-soluble and water-soluble particles for application in photosensitive polymers and tetraethylorthosilicate (TEOS) water based sol-gels, respectively. Since the procedure is more or less similar for both types of particles, only the preparation of the water-soluble particles will be discussed in this section. More information on the preparation of the cyclopentanone-soluble particles can be found in the article of Stouwdam et al. (3).

We dissolved 0.126g of NaF as the fluorine precursor in 35ml of water. To this solution we added 2.0g of citric acid, $HOC(COOH)(CH_2COOH)_2$, followed by neutralizing the solution with NH_4OH until a pH of 7 and heating it to 75ºC. The molecular structure of citric acid is shown in Figure 1a. In solution, the OH groups loose the hydrogen and become negatively charged. The citrate molecules will encapsulate the LaF_3 particles during growth, determining the final size of the particles and making sure that the particles dissolve well in water.

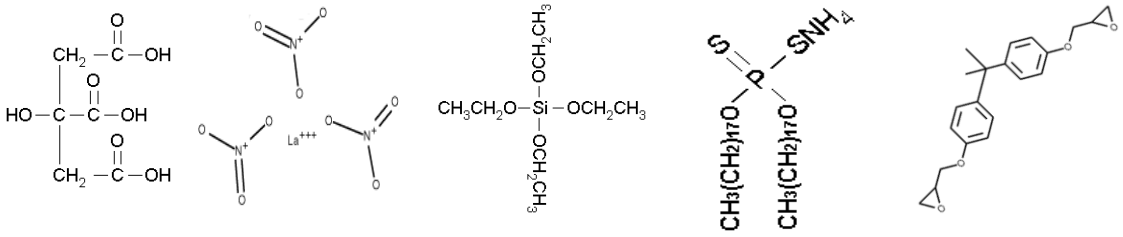

(a) Citric acid (b) $La(NO_3)_3$ (c) TEOS (d) Dithiophosphate (e) BPA di-glycidyl ether

Figure 1: Molecular structures of some of the precursors used in this research.

When the solution reached 75ºC, a 2ml solution of 0.5473g $La(NO_3)_3.6H_2O$ (Figure 1b) and 0.0288g $Er(NO_3)_3.5H_2O$ was added drop wise to serve as the lanthanum and erbium precursors. The ratio between these two precursors determines the final erbium concentration inside the particle, which is 5 atomic percent in this case. In order to synthesize neodymium doped nanoparticles, the erbium nitrate is simply replaced by its neodymium counterpart, $Nd(NO_3)_3.6H_2O$. The reaction was allowed for two hours after which 100ml of ethanol was added to precipitate the citrate incorporated LaF_3:Er

particles that were formed. Finally, the particles were separated by centrifugation at 3500rpm, washed with ethanol and dried under vacuum. The average diameter of the formed nanoparticles is around 6nm as can be seen in Figure 2.

Host materials

As mentioned in the introduction, two types of nanoparticle hosts that can be spin coated are of interest, namely photosensitive polymers and sol-gels. A photosensitive polymer is an interesting material in order to fabricate LaF_3:Nd doped waveguides in a one step lithography process, since polymers have an optical transmission window around 1330nm where the neodymium is active. The sol-gels are more suitable as hosts for the LaF_3:Er nanoparticles, because the inorganic glass structure of the final film can sustain higher annealing temperatures to remove OH bonds that cause absorption in the wavelength region of interest (1530nm) and quench the excited states of the erbium.

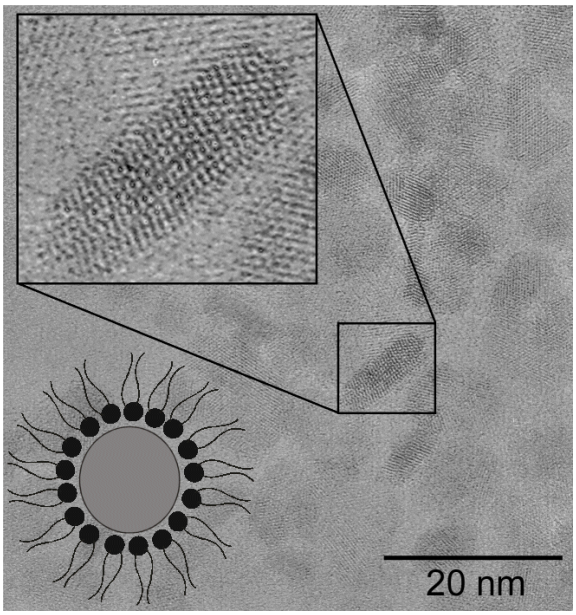

Figure 2: Transmission electron microscope image of LaF_3-nanoparticles.

For the photosensitive polymer we used a form of diglycidyl ether of Bisphenol A (BPA) as the base material (Figure 1e), which is an optically clear material that can be solved in cyclopentanone. Precursors come in a wide range of chain lengths, determining the reactivity and viscosity. The chain length should be chosen such that a dry film is formed after spin coating in order to facilitate contact UV exposure through a photo mask. Additionally, a photo-initiator, adhesion promoter and the LaF_3:Nd nanoparticles are added to the solution. The ammonium di-*n*-octadecyldithiophosphate (Figure 1d) used in the nanoparticle preparation (3) prevents clustering of the nanoparticles. The hydrocarbon tails are extending outward, while the negatively charged sulfur ion adheres to the particle. Figure 2 shows a typical transmission electron microscope (TEM) image of the nanoparticles. In the lower left bottom inset, a schematic representation of a dithiophosphate-encapsul-ated nanoparticle is shown. Depending on the solvent concentration and spinning speed, uniform nanoparticle doped films with a thickness ranging from 500nm to 5µm can be deposited. A 5-minute baking step at 95ºC to remove the solvents is followed by a 1 minute UV exposure step in a standard mask aligner through a chrome mask using standard I-line lithography. The acids, that are generated by the photo-initiator during UV

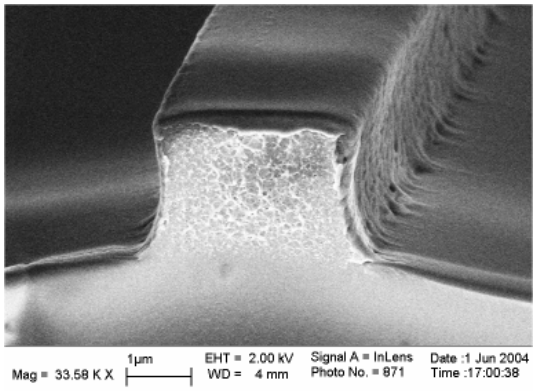

Figure 3: SEM image of a monomode polymer waveguide.

exposure, open up the epoxy groups of the BPA (Figure 1e) during a 2 minute after exposure bake at 95ºC. During this after exposure bake, the reactive epoxy groups will form a cross-linked network. The unexposed parts of the film can be removed with a standard resist developer (RER600, PGMEA). Figure 3 shows a scanning electron microscope (SEM) image of a monomode optical waveguide.

The inorganic SiO_2 host was prepared through the sol-gel method, based on the procedure reported by Xiang et al. (4). Around 80mg of the citrate incorporated LaF_3:Er particles (preparation described earlier) were dissolved in 1ml of water. To this, we added 3ml of tetraethylorthosilicate (TEOS, Figure 1c) as the precursor for SiO_2 and 7.8ml ethanol. The pH was brought to 2 by adding a few drops of concentrated HCl. This solution was spin coated onto a silicon wafer yielding uniform films. Two heat treatment steps at 100ºC and 300ºC were carried out to form a crack free SiO_2 network. A spinning speed of 3600 rpm results in a film thickness of 167nm after the two baking steps. Additional annealing for 1.5 hours at 1100ºC causes further densification of the film, resulting in a thickness of 147nm. Crack free film stacking has been demonstrated this way up to 6 layers, resulting in 1μm thick films (5).

RAYLEIGH SCATTERING

It is well known that refractive index disturbances will cause scattering of light. This so called Mie-scattering (in case of spherical shapes) can be treated as Rayleigh scattering in case the size of the spheres is small compared to the wavelength of the incident light ($r<<\lambda$). The Rayleigh scattering cross section, σ_{Rayl}, at wavelength λ and particle radius r of a particle with refractive index n_p, embedded in a host with refractive index n_h, is given by (6):

$$\sigma_{Rayl} = \frac{8}{3}\left(\frac{2\pi n_h r}{\lambda}\right)^4 \cdot \left(\frac{\left(\frac{n_p}{n_h}\right)^2 - 1}{\left(\frac{n_p}{n_h}\right)^2 + 2}\right)^2 \pi r^2 \qquad [\mathrm{m}^2] \qquad [1]$$

By multiplication of the scattering cross section with the fill fraction η of the nanoparticles and subsequently dividing this by the particle volume, one can obtain the total Rayleigh scattering coefficient (7) in cm^{-1} and the loss in dB/cm (5):

$$a_{Rayl} = \frac{3\eta\sigma_{Rayl}}{4\pi r^3}\ [\mathrm{m}^{-1}] \qquad \alpha_{Rayl} = \frac{\log(e)\cdot a_{Rayl}}{10}\ [\mathrm{dB/cm}] \qquad [2\text{-}3]$$

The λ^{-4} dependency and the strong dependency on the particle radius of $\sim r^6$ can be clearly seen in Figure 4 for LaF_3 nanoparticles (n_p = 1.59) embedded in a silica host matrix (n_h = 1.45) and a BPA based polymer host (n_h = 1.58), both having a volume fill fraction of η = 0.1. From Figure 4 it can be concluded that the scattering losses of LaF_3:Er dispersed in SiO_2 are still acceptable in case of our nanoparticles with r = 3nm. The scattering losses in case of the nanoparticles dispersed in the polymer film can be neglected, since both their refractive indices are matched as can be seen in the top graph of Figure 4.

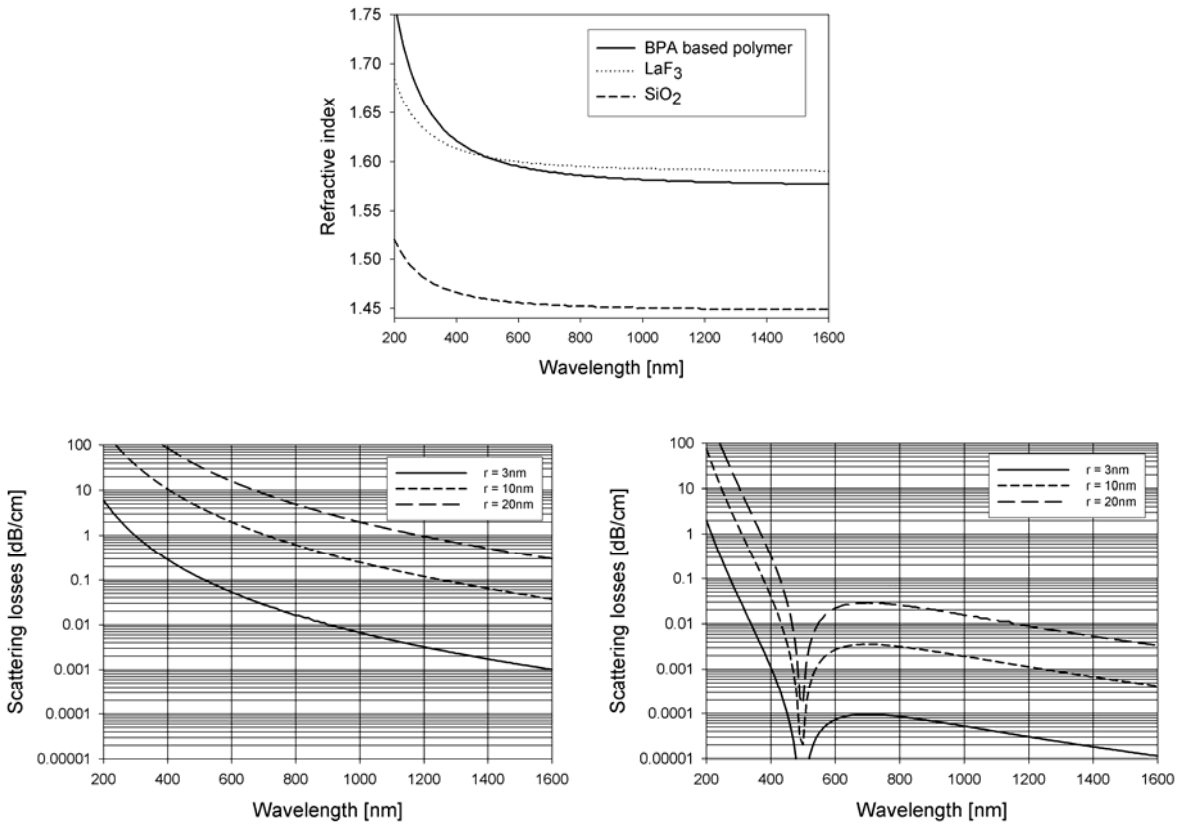

Figure 4: Refractive index versus wavelength for BPA, LaF_3 and SiO_2 (top) and the theoretical Rayleigh scattering losses for LaF_3 nanoparticles with different sizes in SiO_2 (bottom-left) and BPA based polymer (bottom-right), respectively.

LOSS MEASUREMENTS OF POLYMER FILMS

A dual prism setup has been used to determine the polymer thin film optical losses over a broad wavelength range. A halogen lamp was used as a broad wavelength source, emitting a continuous spectrum ranging from 400-1700nm. The white light from this source was fed into a fiber bundle with a large diameter of 6mm. At the other end of the fiber bundle the light is focused onto the corner of a 60-30-90 degree prism using a positive lens with a small focal length (20mm). The 90-degree corner of the prism is being pressed onto the sample, creating a thin air gap to facilitate evanescent field coupling into the thin film. Because the wavelengths are supplied over a broad range of angles using the positive lens, the coupling condition [4] is satisfied for all wavelengths.

$$N_{eff} = n_p \sin\left[\alpha_p + \arcsin\frac{\sin\theta}{n_p}\right] \qquad [4]$$

Where N_{eff} is the effective index of a particular optical mode in the thin film, n_p is the refractive index of the prism, α_p represents the base angle of the prism and θ is the external angle at which the light enters the prism. After a certain distance d, another prism is being pressed onto the sample in order to couple the propagating light out of the film again. The light is then focused onto another fiber bundle and fed into a photo spectrometer (Spectro320 from Instrument Systems). Figure 5 shows a schematic drawing of the measurement setup.

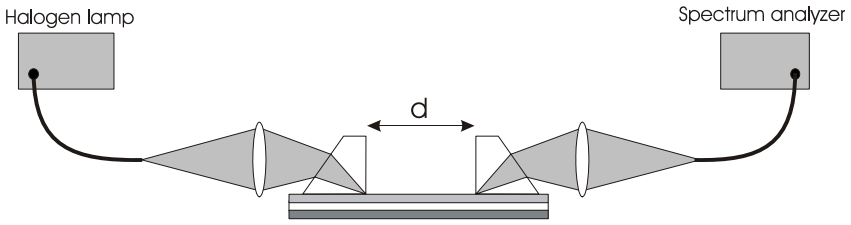

Figure 5: Schematic drawing of the dual prism loss measurement setup.

After each spectral measurement, the transmission spectrum is stored and the outcouple prism is moved with a step Δd towards the incouple prism, after which a next transmission spectrum is being recorded. This procedure is repeated several times, until the prisms are in closest proximity to each other. Once a series of spectra has been recorded, the data can be processed to determine the thin film optical losses as function of wavelength. Figure 6 shows an example of this procedure in the wavelength range 1100nm-1300nm where absorption peaks due to CH bonds are located.

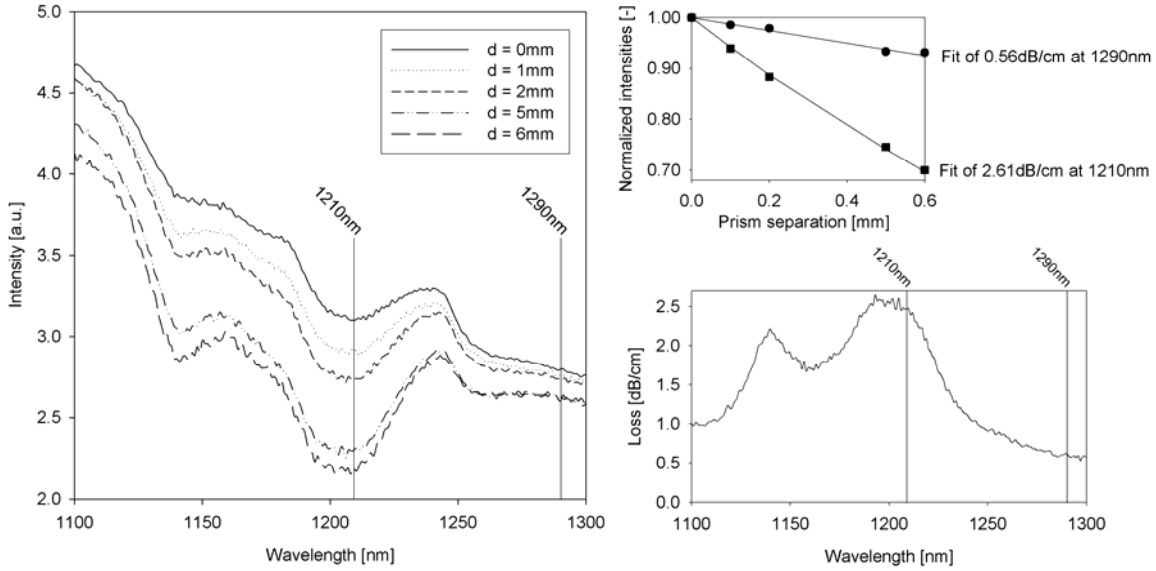

Figure 6: Optical loss calculations using a range of transmission spectra. As an example, the theoretical fits are shown for two wavelengths (1210nm and 1290nm) around the 3rd overtone absorption band of the CH-bonds that are present in the polymer.

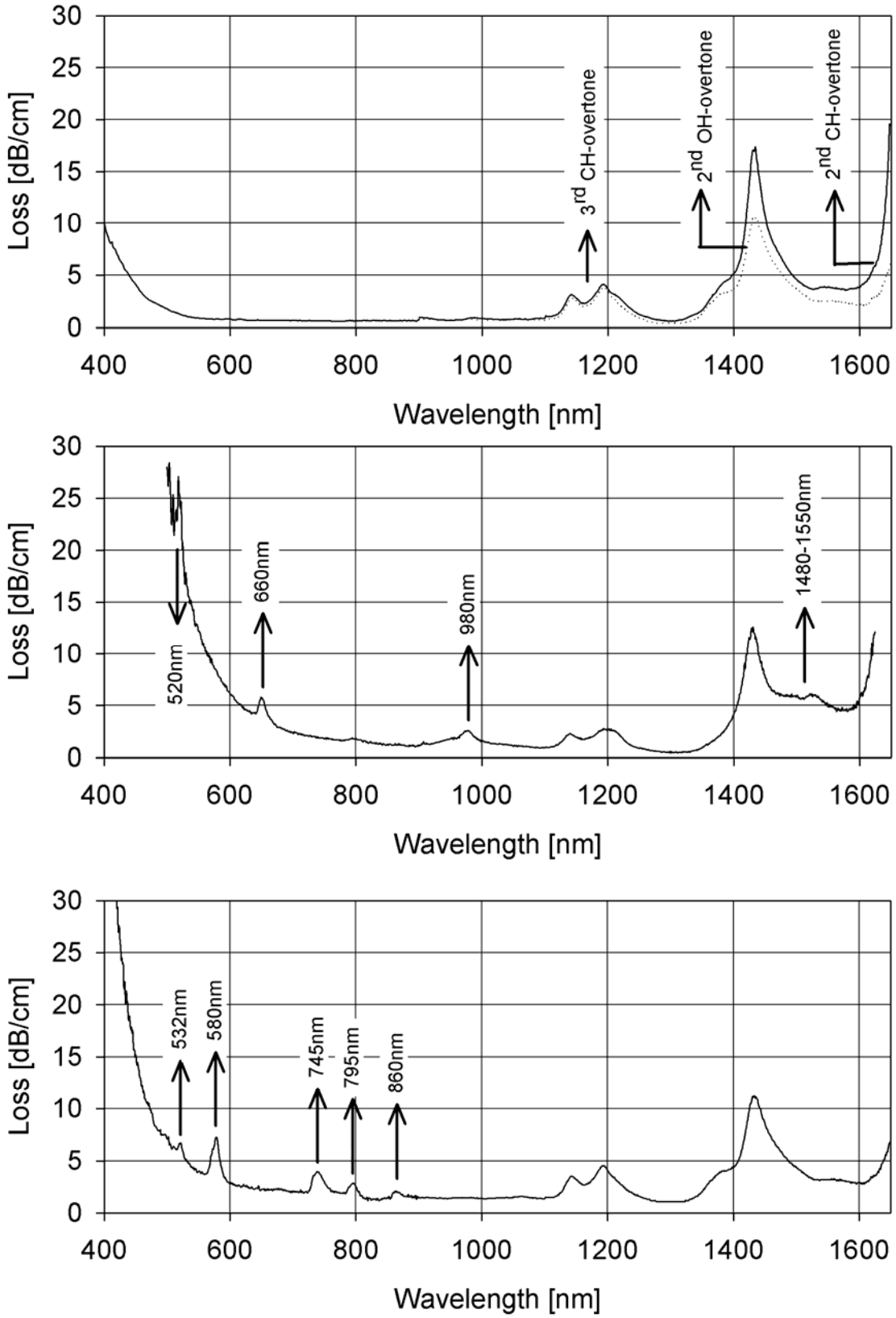

Figure 7: Optical loss spectra of an undoped photosensitive polymer thin film (top), and of the same polymer dispersed with erbium (middle) and neodymium (bottom) doped LaF_3 nanoparticles, respectively.

In Figure 7, the optical losses are shown of an undoped photosensitive polymer thin film (top), and the same polymer dispersed with erbium (middle) and neodymium (bottom) doped LaF_3 nanoparticles, respectively.

The exponential loss (8) of the polymer films can be clearly observed at short wavelengths in Figure 7, as well as the 3rd CH-overtones around 1175nm and the 2nd OH-overtone around 1438nm, in good agreement with the overtones described by Groh (9). In case of the undoped polymer film, the CH absorption remains constant while the OH absorption decreases (dotted line), as expected, after a short 100ºC-baking step to remove the absorbed water. Furthermore, the typical absorption lines of the erbium (520nm, 660nm, 980nm and 1480-1550nm) and the neodymium (532nm, 580nm, 745nm, 795nm, and 860nm) are clearly shown. The loss due to the erbium and neodymium can be used to determine the rare earth concentration, N (in cm^{-3}), of the film by dividing the wavelength dependent loss, $a(\lambda)$ (in cm^{-1}), by the absorption cross section, $\sigma(\lambda)$ (in cm^2), of the corresponding rare earth ion. Scattering of the nanoparticles (n=1.59) does not cause the increased absorption at shorter wavelengths, since its refractive index is matched by the polymer (n=1.58), but by UV absorption of the yellowing ligands, which are attached to the nanoparticles. This is also indicated by the fact that the absorption tail at the short wavelengths has an exponential behavior instead of the λ^{-4} behavior in case of Rayleigh scattering.

LIFETIME ENHANCEMENT IN ANNEALED SILICA FILMS

As mentioned earlier, in the case of erbium, the CH and OH bonds that are present in both the polymer and sol-gel based films cause background losses in the wavelength region of interest and the latter is a serious energy quencher of the excited state of the erbium ions. The glassy SiO_2 films prepared by the TEOS based sol-gel process can be annealed at high temperatures in order to anneal out the OH and CH bonds. Figure 8 shows the erbium decay curves of the LaF_3:Er doped SiO_2 (previously discussed) after annealing for 12 hours at temperatures of 600ºC and 800ºC, respectively. Furthermore, the decay curves are shown for TEOS based SiO_2 films, where the erbium ions were directly incorporated into the SiO_2 matrix by adding the $Er(NO_3)_3.5H_2O$ salt to the sol-gel instead of the LaF_3:Er nanoparticles. The samples were excited with 5ns pulses from a Quantel Nd-YAG laser at 488nm.

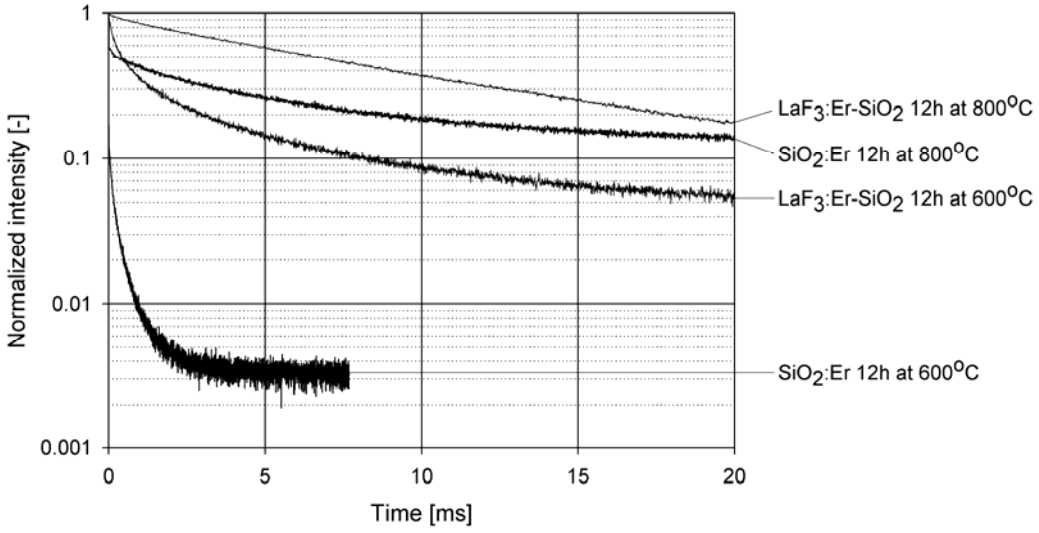

Figure 8: Erbium decay curves of erbium doped TEOS based silica and erbium doped LaF_3 nanoparticles dispersed in TEOS based silica, annealed for 12h at 600ºC and 800ºC.

The excited state lifetime of the erbium ions, defined as the time where the emitted photon intensity reaches the 1/*e* value of the normalized intensity at $t = 0$s, can be derived from the decay curves of Figure 8. The fitted results are listed in Table I.

Table I: Lifetime values with the relative percentages of the decay components in brackets.

Temp	LaF_3:Er-SiO_2 films		SiO_2:Er films	
	τ_1 ms (%)	τ_2 ms (%)	τ_1 ms (%)	τ_2 ms (%)
600 °C	7.4 (69%)	0.9 (31%)	0.98 (35%)	0.27 (65%)
800 °C	10.9 (95%)	3.9 (5%)	6.0 (70%)	1.2 (30%)

For both annealing temperatures it can be seen that the lifetimes are higher for the samples where the erbium is surrounded by the LaF_3 matrix. This is because the LaF_3 matrix is shielding the erbium from the OH-quenching environment of the SiO_2 host. Furthermore, it is clear that the lifetimes for both samples increase at higher annealing temperatures, indicating a reduction in OH concentration and/or a better crystallinity of the surrounding matrix.

CONCLUSIONS

Erbium and neodymium doped LaF_3 nanoparticles have successfully been synthesized with citrate and dithiophosphate based ligands to make them soluble in water and cyclopentanone, respectively. The rare earth doped nanoparticles were dispersed into a photosensitive (UV-cross linkable) BPA polymer and monomode optical waveguides

were fabricated using standard I-line lithography. Absorption spectroscopy has been carried out on the undoped and doped polymer thin films, revealing a broad range of material properties, like the presence of CH bonds, water absorption, nanoparticle/rare-earth concentration, the electronic absorption edge at short wavelengths and the excluding of Rayleigh scattering by the nanoparticles.

Furthermore, TEOS based sol-gels have proven to be good hosts for LaF_3:Er nanoparticles, since they can be annealed at high temperatures to reduce the OH concentration. The excited state lifetime of the erbium in these samples was increased to 10.9ms, which is high compared to other erbium doped sol-gel based thin films.

Both the organic and inorganic host materials in combination with the rare-earth doped LaF_3 nanoparticles offer the possibility to deposit optically active thin films at low cost. Expensive and time consuming etch processes can be avoided in case of the neodymium doped nanoparticles in combination with the photosensitive polymer using standard I-line lithography. The inorganic sol-gel based films can be used as active cladding materials on top of passive waveguides.

We are currently developing a hybrid photosensitive host material that consists of both silica and hydrocarbon bonds (ceramic/organic) in order to reduce the losses around the 1530nm window.

ACKNOWLEDGEMENTS

The authors would like to thank Remco Nieuwland for preparing the LaF_3:Nd doped polymer thin films. This research is supported by the Freeband Impulse technology program of the Ministry of Economic Affairs of the Netherlands.

REFERENCES

1. A. Polman, *Physica B*, **300**, 78-90 (2001).
2. R. Nieuwland, R.Dekker, L.T.H. Hilderink, M.B.J. Diemeer, K. Wörhoff, J.W. Stouwdam, F.C.J.M. van Veggel and A. Driessen, *Proceedings of the 2004 Annual Symposium IEEE/LEOS Benelux Chapter*, 2-3 December 2004, Ghent University, Belgium, 323-326, ISBN: 9076546061.
3. J.W. Stouwdam and F.C.J.M. van Veggel, *Nano Lett.*, **2**(7), 733-737 (2002).
4. Q. Xiang, Y.Y. Zhou, B.S. Ooi, Y.L. Lam, Y.C. Chan and C.H. Kam, *Thin Solid Films*, **370**, 243 (2000).
5. R.Dekker, V. Sudarsan, F.C.J.M. van Veggel, K. Wörhoff and A. Driessen, *Proceedings of the 2004 Annual Symposium IEEE/LEOS Benelux Chapter*, 2-3 December 2004, Ghent University, Belgium, 295-298, ISBN: 9076546061.
6. A. J. Cox, A. J. DeWeerd, and J. Linden, *Am.J.Phys.*, **70**(6), 620-625 (2002).
7. L. H. Slooff, A. v. Blaaderen, A. Polman, G. A. Hebbink, S. I. Klink, F. C. J. M. v. Veggel, D. N. Reinhoudt, and J. W. Hofstraat, *Appl. Phys. Rev.* **91**(7), 3955-3980 (2002).
8. F. Urbach, *Phys.Rev.,* **92**, 1324 (1953).
9. W. Groh, *Makromol.Chem.*, **189**, 2861-2874 (1988).